Ball Pen Probe in Strongly Magnetised RF Plasmas

B. J. Harris[1], M. Smith[1], S. Murphy-Sugrue[2], J. Harrison[2], J. W. Bradley[1] and P. M. Bryant[1*]

[1] *Department of Electrical Engineering and Electronics, University of Liverpool, Liverpool, L69 3GJ, United Kingdom.*
[2] *Culham Centre for Fusion Energy, Culham Science Centre, Abingdon, Oxon OX14 3DB, United Kingdom.*

E-mail: * pmbryant@liv.ac.uk

Received xxxxxx
Accepted for publication xxxxxx
Published xxxxxx

Abstract

A study of ball pen probes in a rf strongly magnetised plasma is reported for the first time. These probes have been successfully used in fusion plasmas, with magnetic fields up to 2.5 T, to measure the plasma potential. In this paper experimental results of various ball pen designs (2 and 4 mm diameter with flat and conical collectors) are presented up to 0.5 T in a low pressure capacitively coupled rf plasma. A theory of the ball pen probe is developed and shows that the increase of the collector potential (electron shielding region) and plateau region, with collector retraction, requires the electron current to decrease faster than the ion current. Experimentally, it is found that to develop effective electron screening the electron Larmor radius should be smaller than the tunnel internal diameter. Smaller tunnels improve screening due to the tunnel entrance wall sheaths. Inside the tunnel a plateau region forms at 81 mT reducing to a broad peak at higher field strengths. Ion shielding and surface losses (for small tunnel diameters) reduce the collector peak width and maximum potential with increasing magnetic field. Conical collectors were found to increase the length of the plateau region and broaden the peak. Particle in cell simulations were in good agreement with the experimental results with and without the magnetic field. The electron shielding and plateau regions were reproduced but not the broad peak at higher field strengths. Good agreement between both 2 mm ball pen probes and an emissive probe was found only at 81 mT to within 3 V or 1.3 electron temperatures (T_e). For all ball pen probes at higher field strengths ($\geq$ 250 mT) the maximum collector potential underestimated the emissive probe by more than 2.7 T_e (7 V). At these field strengths all ball pen probes agree with each other to within 1.5 T_e (4.1 V). Possible reasons for these disagreements are discussed.

Keywords: Ball pen probe, plasma potential, magnetised plasma, RF plasma, low temperature non-thermal plasma

1. Introduction

Ball pen probes (BPPs) have advantages over other methods of measuring the plasma potential. Their simple and robust design, combined with simple electronics, makes them an attractive alternative to conventional methods such as Langmuir probes. BPPs are unlikely to melt or erode in fusion plasmas and, due to their inherent electron shielding, are less sensitive to electron temperature fluctuations (Silva *et al.* (2015)). Recently, ball pen probes have been successfully used to directly measure the plasma potential in a Heliotron (Michael *et al.* (2017)) and in various tokamaks such as ASDEX upgrade (Adámek *et al.* (2009), Horacek *et al.* (2010), and Müller *et al.* (2011)), COMPASS (Adámek *et al.* (2014)), IR-T1 (Meshkani *et al.* (2015)) and ISTTOK (Silva *et al.* (2015)). By combining two BPPs the electric field and its fluctuations have been measured in the MAST tokamak (Walkden *et al.* (2015)). In recent developments both toroidal and poloidal electric field fluctuations, which are used to obtain the Reynolds stress tensor, have been measured by using ball pen probes in the COMPASS tokamak (Grover *et al.* (2017)). A novel variation of the BPP design, called a bunker probe, is almost independent of the magnetic field orientation (Costea *et al.* (2016)).

Developed by Adámek and co-workers (Adámek *et al.* (2004)), the ball pen probe consists of an insulating tube (see figure 1) within which is placed a moveable conducting collector. This floating collector is isolated from ground by a high impedance buffer. The collector can be recessed (operating as a BPP) or protruded where it can be used as a

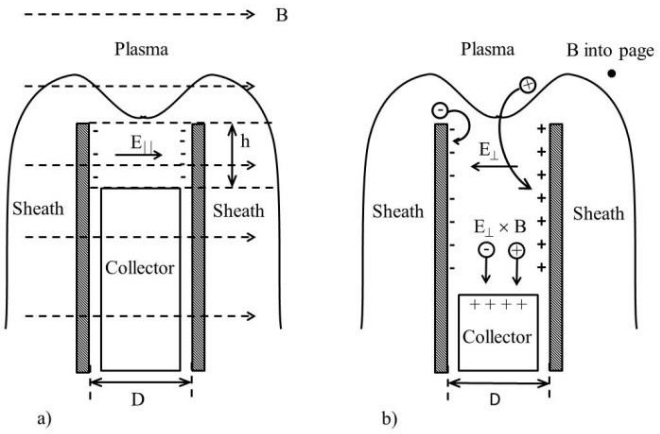

Figure 1 Schematic of the ball pen probe (BPP). In a) a BPP, of internal diameter D, is orientated perpendicular to the magnetic field lines. A collector is recessed into the tunnel at depth h. In b) wall charging due to opposite gyro-orbits of ions and electrons causes $E_\perp \times B$ drifts towards the recessed collector.

Langmuir probe. The BPP is orientated perpendicular to the magnetic field lines (see figure 1). Two main geometries of the collector have been used such as the flat (Walkden *et al*. (2015)) and the conical collector (Adámek *et al*. (2004)).

The principle of operation relies on the fact that the much larger ion Larmor radius enables ions to reach the recessed collector whereas the electrons, due to their much smaller orbit, do not. This interpretation requires both species to be sufficiently magnetised. In practice the collector is recessed at depths corresponding to about one ion Larmor radius or deeper. The plasma potential, V_p, is then given by the following equation assuming a collisionless thin sheath:

$$V_p - V_C = T_e\,\alpha \;\text{ with }\; \alpha = ln(R) = ln\left(\frac{I_{e(sat)}}{I_{i(sat)}}\right). \qquad (1)$$

Here, V_C is the floating collector potential, T_e is the electron temperature (in electron volts) and $I_{i,e(sat)}$ is the probe's saturation current for ions (i) and electrons (e). According to equation 1 when $I_{e(sat)} = I_{i(sat)}$ then $\alpha = 0$ and $V_p = V_C$. In general it is found that $\alpha > 0$ at the plateau and depends on the probe design. In fusion plasmas $\alpha = 0.6 \pm 0.3$ (Silva *et al*. (2015)) so that this indirect method requires knowledge of T_e. Experimentally α is obtained by linear extrapolation of the ion (electron) saturation current to the collector potential.

This simple model has been successfully applied to BPPs and Langmuir probes in fusion plasmas. Relatively few studies have used the ball pen probe in magnetised low temperature plasmas. Adámek *et al*. (2012 & 2013) compared the BPP potential with a protruded BPP (operated as a Langmuir probe) and a separate conventional Langmuir probe with magnetic field strengths up to 72 mT. Good agreement was obtained in a DC cylindrical magnetron, a linear plasma device and in the torsatron TJ-K. Bousselin *et al*. (2013) conducted ball pen studies in a linear plasma device at pressures of 0.02 to 0.04 Pa and field strengths from 5 to 80 mT in argon and helium plasmas. Comparison with the plasma potential, obtained from the protruded collector and an emissive probe, also showed good agreement. The authors concluded that for plasma potential measurement the electron Debye length, λ_{De}, to tunnel internal diameter, D, ratio should be sufficiently large. Furthermore, r_{Le} must be greater than D where r_{Le} is the electron Larmor radius. The second conclusion is inconsistent with the simple ball pen model which requires $D > r_{Le}$. A further study was performed by Zanáška *et al*. (2015) in a cylindrical magnetron with field strengths up to 40 mT and pressures from 1 to 20 Pa in argon. In their experiments the ball pen probe agreed with a cylindrical Langmuir probe to within 1.5 V. The main conclusion of this work is that the BPP becomes operational when the field to pressure ratio, B / P, exceeded 10 mT / Pa. In these plasmas the magnetic field is sufficiently weak so that the ions are relatively unmagnetised.

Despite the use of BPPs in fusion and in magnetised low temperature plasmas, the underpinning theory is relatively undeveloped. Recently, a fully 3D (3D3V) PIC simulation of a BPP in fusion relevant conditions ($T_{e,i}$ = 60 eV, B = 0.54 T, $n_e = 6.5 \times 10^{17}$ m^3) was performed (Murphy-Sugrue *et al.* (2017)). The higher mobility of the electrons, compared to the ions, causes a net negative charge build-up on the tunnel wall and a parallel electric field $E_{||}$ in the direction of the magnetic field (figure 1a). Perpendicular to the magnetic field the opposite orbital direction of the ions and electrons causes an electric field $E_\perp$ to develop (see figure 1b). This results in a $E_\perp \times B$ drift of both species into the tunnel. The deposition of net negative charge onto the inner tunnel wall causes the low energy electrons to bounce between the wall sheaths as they drift towards the collector. The continuously decreasing deposition of charge causes the electron density to decrease into the tunnel. Ions can reach the collector if their perpendicular (to the magnetic field) velocity, $v_\perp$, is such that $v_\perp > v_{||}$ (h / D) where $v_{||}$ is the parallel velocity. Typical recession depths are about one ion Larmor radii or greater so that ions are able to reach the collector before colliding with the tunnel wall. Consequently, larger diameter probes have lower α values and float closer to the plasma potential. This is because more ions are able to reach the collector and balance the electron flux which does not change significantly with tunnel diameter. The authors also confirmed that the floating potential of the BPP is offset from the plasma potential by the factor $\alpha\, T_e$.

The aim of this work is to investigate the applicability of the BPP method in a radio-frequency (rf) low temperature low

pressure magnetised plasma. A simple theory of the BPP probe is developed. Results are then presented on several different ball pen probe designs. Experiments were performed at 0.45 Pa in argon over a range of magnetic field strengths up to 0.5 T. The magnetic field strength of 0.5 T is close to those found in the SOL of MAST (Sykes *et al.* (2001)).

2. Theory of Ball pen probe

Consider a recessed planar disc collector filling the interior of an insulated tunnel with an internal diameter D. It is assumed that the probe is immersed in a Maxwellian plasma with no time-varying electric fields. Ion-neutral collisions and ionisation are neglected. Due to the higher electron mobility the interior wall of the tunnel are negatively charged and at floating potential. The positive ions enter the tunnel at x = 0 after being accelerated through the external sheath. Because of symmetry the equipotential surfaces are curved with a potential maximum along the central tunnel axis. This causes the ions to be accelerated towards the walls where they are deposited. It has been observed by Adámek *et al.* (2005) and in this work (see section 4.2.2) that both the ion and electron currents decrease exponentially with retraction depth (x > 0). The ion current is then described by:

$$I_i(x) = I_{io} e^{-\frac{x}{\delta_i}} \tag{2}$$

where I_{io} is the ion current entering the tunnel (at x = 0) and δ_i is the ion attenuation distance. The decreasing electron current, due to continual deposition onto the walls, is given by a similar equation:

$$I_e(x) = I_{eo} e^{-\frac{x}{\delta_e}} \tag{3}$$

where I_{eo} is the initial electron current and δ_e is the electron attenuation distance.

The particle transport down the tunnel results in a potential gradient (Murphy-Sugrue *et al.* (2017)). In general, this can be written in the form $\Delta V_R = I_{net}(x)\, R(x)$ with equivalent tunnel resistance $R(x) = \rho(x)\, x / A$ and net current $I_{net}(x) = I_e(x) - I_i(x)$. Here, $\rho(x)$ is the space charge resistivity with the tube's cross-sectional area given by $A = \pi D^2 / 4$. Note that $R(x) \propto D^{-2}$ and is reduced for larger tunnel diameters. As shown in figure 2 additional voltage drops may be present outside the tunnel, due to the sheath (ΔV_s), and in front of the recessed floating collector (ΔV_C). The potential at the collector, $V_C(h)$, can then be related to the plasma potential, V_p, by:

$$V_C = V_p - \Delta V_s - \Delta V_R - \Delta V_C. \tag{4}$$

For the BPP to directly measure the plasma potential ($V_C = V_p$) the other terms must be made small in comparison to V_p. For large tube diameters ($R \rightarrow 0$) or for thin sheaths, where $D >> \lambda_{De}$, then both ΔV_s, $\Delta V_R \rightarrow 0$. This due to the collapse of the external sheath and the penetration of plasma into the tube. Since the interior of the BPP consists of floating surfaces then $I_{net}(x) \rightarrow 0$ so that ΔV_R may be ignored. This leaves $V_C(h) = V_p - \Delta V_C(h)$ with the BPP measuring the plasma potential if $\Delta V_C(h)$ can be made to be sufficiently small.

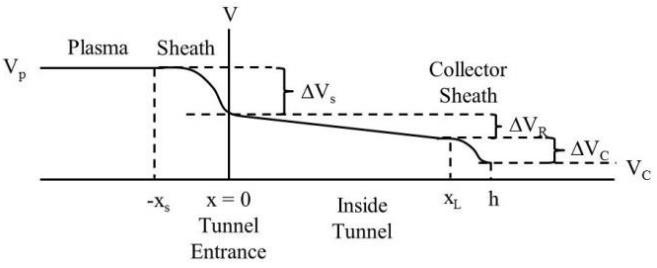

Figure 2 Variation of potential from bulk plasma to the recessed collector at depth h in the ball pen probe. V_p – plasma potential, ΔV_S – sheath potential drop of width x_s, ΔV_R – resistive potential drop, ΔV_C – collector sheath potential drop of width h - x_L, V_C – collector potential.

The electric field set-up by the floating collector at depth h repels the low energy electrons and accelerates the positive ions to the collector. The balance of electron and ion currents at the collector determines the collector's floating potential (relative to ground), $V_C(h)$. The collector's floating potential is given by the solution of:

$$I_i(h) = I_e(x_L) e^{-\frac{V_L(x_L) - V_C(h)}{T_e}}$$

where $V_L(x_L)$ is the local space charge potential in the tunnel (at depth $x_L < h$) as shown in figure 2. For distances h - x_L << δ_i and under collisionless conditions the conservation of ion flux in the vicinity of the collector ensures that $I_i(x_L) = I_i(h)$. Rearranging and solving for $\Delta V_C(h) = V_L(x_L) - V_C(h)$ leads to:

$$\Delta V_C = T_e \ln\left(\frac{I_{e(x_L)}}{I_{i(h)}}\right). \tag{5}$$

Substituting equations (2 – 3) into equation (5), with $\delta_{i,e}$ as functions of h and $x_L \approx h$ (for $h - x_L << h$), then yields:

$$\Delta V_C(h) = T_e \left[\ln\left(\frac{I_{eo}}{I_{io}}\right) + h\left(\frac{1}{\delta_i} - \frac{1}{\delta_e}\right)\right]. \tag{6}$$

The variation of collector potential with h can be obtained by substituting (6) into (4), with $\Delta V_s = \Delta V_R = 0$, to obtain:

$$V_C(h) = V_p - T_e \left[\ln\left(\frac{I_{eo}}{I_{io}}\right) + \left(\frac{1}{\delta_i} - \frac{1}{\delta_e}\right) h\right]. \tag{7}$$

The term in square brackets is α (see equation 1). Since the dependence of $\delta_{i,e}$ on h is not known a rigorous analysis is not possible. However, the essential features of the reported experimental data can be obtained if $\delta_{i,e}$ is assumed constant. Three cases are immediately apparent in equation (7): a) $\delta_e >> \delta_i$, b) $\delta_e << \delta_i$ and c) $\delta_e = \delta_i$. In the first case $dV_C / dh = -T_e / \delta_i$ with V_C decreasing with increasing retraction depth into the tunnel as shown in figure 3a. In an unmagnetised non-thermal plasma (*i.e.* $T_e >> T_i$) the tunnel wall charges up negatively reducing the electron loss to the walls. Positive ions are accelerated to the walls increasing their loss so that $\delta_e >> \delta_i$. In the second case $dV_C / dh = T_e / \delta_e$ and V_C increases with increasing retraction depth (see figure 3b). The diffusion coefficient across field lines reduces with increasing magnetic field since $D_\perp \propto B^{-2}$. In addition $D_\perp \propto m^{1/2}$ (with m the particle mass) so electron diffusion is drastically reduced compared to the ions. The increased difficulty of electrons to move down the tunnel with increasing field is equivalent to a reduced δ_e such that $\delta_e << \delta_i$. The screening of the electrons by the magnetic field increases the surface charge on the collector thereby increasing it's potential. This is similar to the operation of gridded Retarding Field Analysers (RFAs) in which the magnetic field's role is replaced by an electron repelling grid (Elmore *et al.* (2012)). Ideally, in the absence of electrons the positively charged collector will repel all positive ions. The collector then floats at the maximum ion energy which is closely related to the plasma potential. The third case in which $\delta_e = \delta_i$ results in V_C being independent of h. This is unlikely due to the different transport and loss mechanisms of both species.

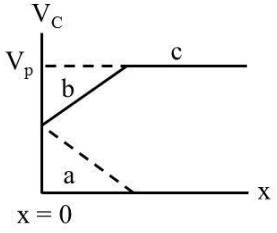

Figure 3 Variation of collector potential, V_C, with depth x. a) Unmagnetised and b) magnetised plasma with $\delta_e > \delta_i$. Screening of electrons by the magnetic field causes the collector potential to increase. c) Plateau region with $V_C = V_p$ (plasma potential).

In strongly magnetised plasmas as the collector is retracted the collector voltage increases until a plateau or peak is reached (see figure 3c). In experiments the collector potential at the plateau is taken to be the plasma potential. Differentiating equation (7) with respect to h with $\delta = f(h)$ gives:

$$\frac{dV_C}{dh} = -T_e\left(\frac{1}{\delta_i} - \frac{1}{\delta_e} + h\left[\frac{1}{\delta_e^2}\frac{d\delta_e}{dh} - \frac{1}{\delta_i^2}\frac{d\delta_i}{dh}\right]\right).$$

For a plateau (or peak) to form within the tunnel (at recession depth h_{pl}) then $dV_C / dh = 0$ which leads to:

$$\frac{1}{\delta_i} - \frac{1}{\delta_e} = \frac{h_{pl}}{\delta_i^2}\frac{d\delta_i}{dh} - \frac{h_{pl}}{\delta_e^2}\frac{d\delta_e}{dh}. \qquad (8)$$

For a plateau this condition applies for a range of h_{pl} (see figure 3c). From equation (7) the requirement that at the plateau $V_C(h_{pl}) = V_p$ or $\alpha = 0$ results in:

$$\left(\frac{1}{\delta_e} - \frac{1}{\delta_i}\right) h_{pl} = \ln\left(\frac{I_{eo}}{I_{io}}\right). \qquad (9)$$

Substituting equation (8) into (9) gives the retraction depth of the plateau region within the tunnel:

$$h_{pl} = \sqrt{\frac{\ln\left(\frac{I_{eo}}{I_{io}}\right)}{\left(\frac{1}{\delta_e^2}\frac{d\delta_e}{dh} - \frac{1}{\delta_i^2}\frac{d\delta_i}{dh}\right)}}. \qquad (10)$$

In non-thermal and fusion plasmas $I_{eo} > I_{io}$ resulting in a constant positive numerator in equation (10). It can be seen that both δ_i and δ_e cannot both be constants or be equal since then $h_{pl} \to \infty$. Given that h_{pl} is both real and positive, so that the plateau region is inside the tunnel, then this requires $\delta_e^{-2}\, d\delta_e/dh > \delta_i^{-2}\, d\delta_i/dh$. Integrating both sides of this inequality yields the result $\delta_i > \delta_e$ so that the electron current decreases at a faster rate than the ion current over the plateau region. Note that this model assumes some electron current will always reach the collector due to the floating condition of equation (5) despite the screening by the magnetic field. This is possible because the increased positive charge on the collector sets up an accelerating electric field for the electrons. The electron current at the collector also means that $V_C(h_{pl}) < V_p$. In a strong magnetic field, such that $I_e(h_{pl}) = 0$ over the plateau region, and under collisionless conditions the collector will float at the maximum ion energy so that $V_C(h_{pl}) = V_p$. It can be seen that throughout the region of increasing V_C (from the tunnel entrance) and the plateau region the electron current must decrease at a faster rate than the ion current.

3. Experimental Set-up

As shown in figure 4 a radio-frequency (rf) argon plasma is generated inside a parallel plate capacitively coupled cell. The 4 cm diameter driven electrode is 4.5 cm below a similar sized grounded indium tin oxide coated window. A Dressler

Cesar 136 generator supplies rf power at 13.56 MHz to the matching unit and driven electrode. The chamber is pumped to a base pressure of 10^{-5} mbar by a Leybold TURBOVAC 50 turbo-molecular pump backed by a Leybold TRIVAC E2 rotary pump. A wide range gauge (Leybold ITR-90), positioned below the chamber, is used for base pressure and chamber pressure measurement (with field off). The gauge was calibrated with a Baratron (MKS Type 627B) mounted on the chamber in no magnetic field. Argon gas (BOC research grade 99.9995%) is introduced into the chamber by a two stage regulator and a mass flow controller (MKS 1179A). The chamber pressure is set by adjusting the flow rate from a mass flow controller interface unit (MKS PR4000B) and also by adjusting the butterfly valve. The aluminium chamber, 14 cm square by 7.5 cm deep, is placed inside the bore of a Helmholtz coil. The current that produces the magnetic field is generated from a Prüftechnik DC power supply (maximum ratings 120 V_{DC} and 1.6 kA_{DC}) and is coupled to a stack of 6 series connected electromagnets. Each magnet (encased in a phenolic enclosure) contains a coil of hollow copper tubing through which chilled water (down to 12 ^{o}C) is passed. The resulting vertically aligned magnetic field (up to 0.5 T) varies less than 0.3 % over the driven electrode.

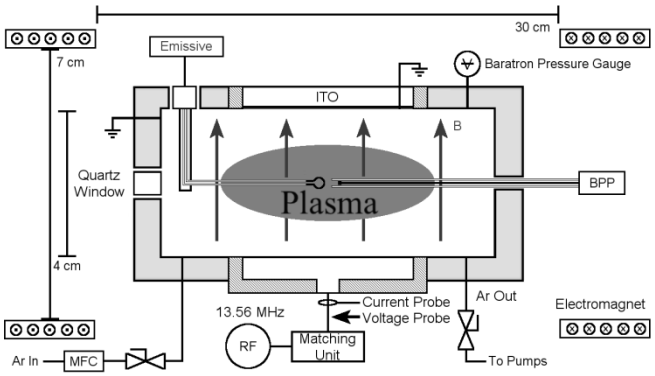

Figure 4 Schematic of the experimental set-up. The plasma chamber is placed inside a Helmholtz coil. Diagnostics include a ball-pen probe (BPP), an emissive probe and an optical probe (not shown - inserted in BPP port). MFC – mass flow controller, ITO – glass coated with indium tin oxide (grounded).

An optical probe based upon a design by Du *et al.* (2010) was used to measure the electron density and temperature. This was inserted into the same port as the BPP being about halfway between the electrodes. This consisted of a 6.35 mm (outer diameter) ceramic tube inserted into the chamber through an o-ring seal. Outside the chamber a converging achromatic lens attached to the tube focuses the plasma emission into a 400 μm optical fibre (Thor Labs, 0.37 numerical aperture). The optical fibre is then passed into an f# matcher (Oriel 77529) and into a ¼ m diffraction grating spectrometer (Oriel MS260l) with an Andor iStar 334T ICCD camera. The whole system was absolutely calibrated with a Newport NIST traceable quartz tungsten halogen (QTH) ribbon lamp (model 63350). The electron density and temperature was obtained using the Corona model (Fantz (2006)). According to the McWhirter criterion this spectroscopic model is valid provided that $n_e < 1.6 \times 10^{18} T_e^{1/2} E^3 m^{-3}$, where E is the energy between electron transition states. For the ArI 750 nm transition used here E = 1.65 eV (Cullen (2015)). With T_e = 3 eV then $n_e < 1.2 \times 10^{19}$ m^{-3}. With n_e typically much less than this (see section 4) this criterion is easily satisfied.

An emissive probe is used to measure the plasma potential (Sheehan and Hershkowitz (2011)) and to compare to the BPP probe. It consists of a loop of 25 μm diameter thoriated tungsten wire (Goodfellows 0.6% Th). The loop is push fitted into two ceramic tubes containing copper rods (recessed by 5 mm) with approximately 1 cm length exposed to the plasma. Heating current is provided by a 50 Hz mains powered variable and fixed step-down transformer as used previously by Mishra *et al.* (2010). The probe voltage is measured by a 100 MΩ resistor connected to a centre tap of the fixed transformer. This ensures that the potential in the middle of the filament is measured. A 10 MΩ voltage probe is connected to the resistor forming a 11:1 potential divider. The probe's floating potential, in the limit of strong emission, is then measured on an oscilloscope. This method is valid in magentised plasmas provided the electron Larmor radius is larger than the wire radius (Sheehan and Hershkowitz (2011)). This ensures that the emitted electrons do not return to the wire filament over their gyration orbit. For this wire diameter the limit is reached at 500 mT. The wire loop is aligned perpendicular to the field lines to ensure that the emitted electrons can escape. The floating point method in the limit of strong emission has been used in many magnetised plasmas to obtain the plasma potential (Sheehan and Hershkowitz (2011)). The emissive probe wire loop was positioned at approximately 1 cm from the BPP tube opening.

Several different designs of the BPP collector and tunnel are shown in table 1. An alumina ceramic tube was used with stainless steel collectors. For each probe the ceramic tube was fixed to the chamber wall. The collector was screwed to a connector pin attached to a 50 Ω screened coaxial cable (1 pF / cm) placed inside a 6.35 mm (outer diameter) stainless steel tube. Epoxy resin was used to fix the pin which also acts as a vacuum seal. The stainless steel tube was passed through an o-ring sealed port on the chamber wall. Outside the chamber the tube was fixed to a movable translation stage. This was used to move the tube assembly and collector inside the fixed ceramic tube. Inside the chamber the ceramic tube extended so that its open end was positioned in the

centre of the chamber halfway between the electrodes. The 2 mm BPP inner diameter (table 1) is similar to that used by Zanaska *et al.* (2015) in their experiments. The importance of a high impedance buffer to measure the collector voltage has been pointed out by several authors (Adámek *et al.* (2013), Bousselin *et al.* (2013) and Zanáška *et al.* (2015)). Following Zanáška *et al.* (2015) a voltage follower using a Texas Instruments op-amp (OPA452) with input impedance of 10^{13} Ω was used.

	Flat	Conical	Flat	Conical
Tube ID (mm)	2	2	4	4
Tube OD (mm)	3	3	5	5
Collector Diameter (mm)	2	2	3.9	3.9
Apex Height (mm)	-	1.5	-	3.5

Table 1 Dimensions of the ball pen probes used in the experiments.

4. Results and Discussion

4.1. Optical Emission Spectroscopy Line averaged argon emission from the 488 nm ion and the 750 nm neutral lines were used to obtain the electron density and temperature with the optical probe. The experimental conditions are the same as those for the ball pen measurements (*i.e.* 10 W at 0.45 Pa). The results are shown in table 2 which also lists other relevant plasma parameters. The electron and ion mean free paths are for collisions with argon neutrals. The ions and neutrals are assumed to be at room temperature (T_i = 0.025 eV) and the ion mean free path and collision frequency were obtained from the zero-field mobility ($\mu_0 = 10^{-4}$ $m^2s^{-1}V^{-1}$ at 10^5 Pa and 273.15 K) (McDaniel and Mason (1970)) corrected for pressure. Electron scattering cross-sections were taken from Lieberman and Lichtenberg (1994) assuming T_e = 3 eV for all field strengths. The Hall parameter is defined here as $\beta_{i,e} = \omega_{i,e} / 2\pi\upsilon_{i,e}$. Here $\omega_{i,e}$ is the ion (electron) Larmor frequency, $\upsilon_{i,e} = v_{i,e} / \lambda_{i,e}$ is the collision frequency, $v_{i,e}$ the average thermal velocity and $\lambda_{i,e}$ the collision mean free path. The Hall parameter represents the number of gyro-orbits completed between collisions with heavy neutrals. In these calculations the thermal velocity is obtained using $v_{i,e} = [8eT_{i,e} / (\pi m_{i,e})]^{1/2}$.

4.2. Ball pen probe h - scans For all h-scans the BPP was first fully extended (with h = 5 mm) into the plasma and then retracted into the tunnel. The emissive probe was positioned out of the way by the chamber wall. The conical probe was considered flush (*i.e.* h = 0) when its tip was level with the end of the ceramic tube. Ball pen measurements were found to be repeatable to within 1 V for all field strengths (2 mm conical BPP).

Pressure (Pa)	P	0.45			
Electron mean free path (cm)	λ_e	20.44			
Ion mean free path (cm)	λ_i	0.40			
Magnetic field (mT)	B	0	81	250	500
B / P (mT / Pa)		0	180.00	555.56	1111.11
Electron temperature (eV)	T_e	2.70	2.40	2.70	2.90
Electron density (10^{16} m^{-3})	n_e	4.10	7.00	3.80	0.70
Electron Debye length (μm)	λ_{De}	60.33	43.53	62.67	151.32
Electron Larmor radius (μm)	r_{Le}	-	72.77	25.01	12.96
Ion Larmor radius (mm)	r_{Li}	-	2.01	0.65	0.33
Electron Hall parameter	β_e	-	447.12	1380.02	2760.03
Ion Hall parameter	β_i	-	0.31	0.97	1.94

Table 2 Parameters for the experimental conditions used for the ball pen measurements. Plasma parameters are based on optical probe measurements of electron temperatures and densities.

4.2.1 Ball pen probes: diameter 2 mm Figure 5 shows axial scans (position denoted by h) of the collector potential for the 2 mm diameter ball pen probe with flat (figure 5a) and conical (figure 5b) collectors. For both probes at 0 mT the collector potential is almost constant for h > 3 mm. Here, the collectors behave as cylindrical Langmuir probes with similar floating potentials of 6.9 V (flat) and 8.0 V (conical). With increasing magnetic field, up to 8 mT, the floating potential decreases to around - 2 V for both collectors. For an ideal cold planar probe the floating potential, V_f, is related to the plasma potential, V_p, by equation 1 (with $V_C = V_f$). Since the logarithmic term does not vary strongly with magnetic field (T_e remains about the same – see table 2) then $V_f \propto V_p$. This suggests that V_p is also decreasing with increasing magnetic field up to 8 mT.

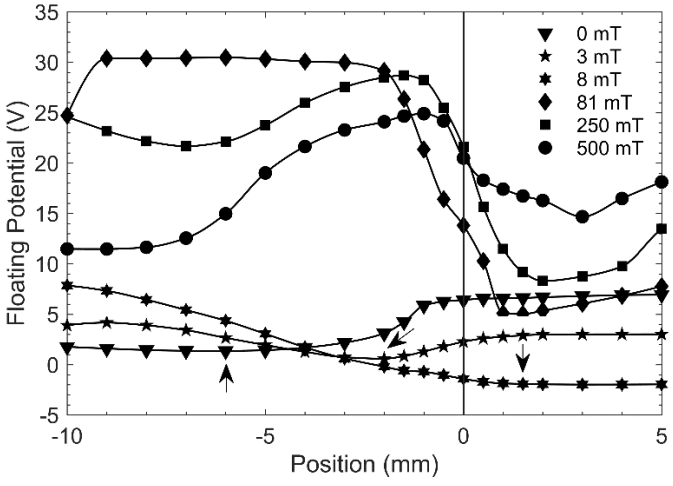

Figure 5a Axial scans for the 2 mm diameter ball pen probe with flat collector at 0.45 Pa and 10 W in argon. Arrows indicate positions of potential minimum.

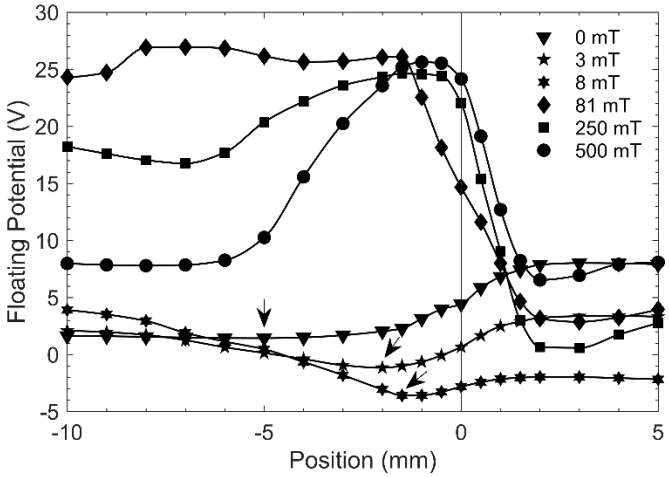

Figure 5b Axial scans for the 2 mm diameter ball pen probe with conical collector at 0.45 Pa and 10 W in argon. Arrows indicate positions of potential minimum.

For h < 3 mm (approximately the tunnel diameter) and at 0 mT the floating potential (V_C) for the flat collector (figure 5a) decreases slowly to h = - 1 mm where it rapidly decreases. The potential reaches a minimum of 1.35 V at h = - 6 mm (indicated by arrow in figure 5a) before slowly increasing to 1.77 V at h = - 10 mm. As the magnetic field increases the minimum potential moves towards the plasma and the gradient dV_C / dh (at depths deeper than the potential minimum) increases.

Unlike the flat collector, the conical collector's floating potential (figure 5b) starts to rapidly decrease at h ≈ 3 mm for fields up to 8 mT. This is comparable to the apex height of 1.5 mm (see table 1) and is likely due to the more rapidly decreasing probe area. Similar behaviour to the flat collector is observed with increasing field strength up to 8 mT inside the tunnel. At 0 mT a potential minimum of 1.44 V is reached at h = - 5 mm (see figure 5b) before slowly increasing to 1.6 V at h = - 10 mm. With increasing field the potential minimum moves towards the plasma and the potential gradient (at deeper depths) increases.

The decrease of the collector voltage with depth is caused by the ion current decreasing at a faster rate than the electron current (see theory section). At depths where h < - 5 mm and for 0 mT the floating potential varies little for both probes. Both electron and ion currents continually decrease within the tunnel so that at sufficiently large depths the stored charge on the collector becomes approximately constant. For both probes the potential gradient (deeper than the minimum) increases inside the tunnel and the potential minimum moves towards the plasma with increasing magnetic field. This is a result of the shielding action of the magnetic field. The electron current then decreases at an increasingly faster rate than the ion current inside the tunnel. For electrons this becomes significant when their Larmor radius is approximately $r_{Le} \approx D$. For the 2 mm BPP, and using the average thermal velocity with T_e = 2.7 eV, the critical field is 12.6 mT in broad agreement with figures 5a and b. This region of increasing dV_C / dh will be referred to as the electron shielding region.

At 81 mT, for both collectors, a steep gradient in dV_C / dh (*i.e.* efficient electron shielding) leads to a well-defined plateau region. For the flat collector (figure 5a), at 81 mT and 500 mT, there is a kink in the potential gradient at the tunnel entrance (h ≈ 0). A similar but less pronounced kink can also be seen for the conical collector (figure 5b) at 81 mT. As the collector is drawn into the tunnel the charging dynamics change from an exposed collector to a partially enclosed collector. The kink is not observed at higher field strengths for the conical BPP because the electron shielding region has moved further out of the tunnel. By assuming $\delta_i >> \delta_e$, so that dV_C / dh = T_e / δ_e, an estimate of the electron attenuation distance, δ_e, can be made. Note that this assumes a weakily varying ion current and attenuation distance over the shielding region. With T_e = 2.4 eV (from table 2) and at 81 mT it is found that δ_e = 0.30 mm (flat) and δ_e = 0.34 mm (conical). An estimate of the ion attenuation distance, δ_i, can also be made by assuming $\delta_e >> \delta_i$ so that dV_C / dh = -T_e / δ_i. In the following the estimate for δ_i is obtained at zero magnetic field over the linear region of the h-scan. Here the electrons are unmagnetised with no magnetic shielding action. For the flat and conical BPP (with T_e = 2.7 eV from table 2) it is found that δ_i = 0.98 mm (flat) and δ_i = 2.86 mm (conical). It is clear that for both flat and conical collectors $\delta_e < \delta_i$ resulting in a positive dV_C / dh gradient which is consistent with the theory. The variation of δ_e (and dV_C / dh) with magnetic field is weak. For example, the flat BPP has δ_e values of 0.31 mm at 250 mT and 0.39 mm at 500 mT.

At 81 mT a plateau region is observed for both collectors extending to h ≈ - 8 mm before the potential decreases. The length of the plateau region is similar for both collectors (*i.e.* flat: 7 mm; conical: 6.5 mm) being about 3.5 r_{Li} (see table 2). A short plateau region (of 2 mm length) was observed by Bousselin *et al.* (2013) in the range 11.4 mT to 68.4 mT, but only for their smaller BPP tunnel of 0.3 mm (internal diameter). At their lowest field strength, and for room temperature argon ions, the ratio r_{Li} / D = 47.7 (D = 0.3 mm). In this case the plateau region is likely to be limited by surface losses which are expected to be more important for smaller tunnel diameters. A longer plateau of at least 5 mm was observed for their larger 1 mm diameter BPP tunnel. Similarly, others have observed plateaus for larger inner diameter tunnels (*e.g.* Zanaska *et al.* (2015): D = 2 mm and Adámek *et al* (2013): D > 2.4 mm). However, these plateau lengths could not be determined due to the limited retraction range. At 250 mT (see figures 5a and 5b) the plateau region reduces to a broad peak with decreasing V_C at large depths (h < - 7 mm). Increasing the field to 500 mT further decreases V_C (at large retraction depths) and for the conical collector

the peak becomes narrower. The shortening of the plateau region and subsequent decrease of V_C implies either a reduction of ion current or an increase in electron current to the collector. The leakage of charge can be dismissed due to the extremely high impedance (10^{13} Ω) of the voltage follower. Since $\delta_e < \delta_i$ throughout the electron shielding and plateau regions (otherwise the electron shielding and plateau regions will not form) it is unlikely that the decrease is caused by electrons. However, ionisation within the tunnel can cause an increase in the electron current to the collector. Taking the maximum ionisation cross-section for Ar ($\sigma_z = 3 \times 10^{-20}$ m^2 (Lieberman and Lichtenberg (1994)) at 0.45 Pa gives an ionisation path length of $\lambda_z = 30.67$ cm. Since $\lambda_z >>$ 5 mm (approximate width of decreasing region) then ionisation cannot be causing the collector voltage to decrease. For $dV_C / dh < 0$ then it follows from the theory that $\delta_e > \delta_i$. The ion current decreases at a faster rate than the electron current leading to the reduction in collector voltage. The reduction of ion current can be caused by surface losses as ions are accelerated towards the negatively charged wall and cross-field diffusion. The cross-field diffusion coefficient for ions can be written as $D_{\perp i} = D_n / [1 + (2\pi\beta_i)^2]$ where D_n is the zero-field diffusion coefficient and β_i is the ion Hall parameter. At 81 mT and 250 mT it can be shown (using table 2) that D_n is reduced by a factor of 4.8 at 81 mT and 38.2 at 250 mT. Furthermore, for the 2 mm BPP (flat and conical) the ratio r_{Li} / D for $B \geq 81$ mT is ≤ 1 for room temperature ions. The decrease of the collector voltage, after the maximum has been reached, can be attributed to the reduced cross-field diffusion as well as surface losses which causes $\delta_i < \delta_e$. This region of decreasing V_C with increasing h (into the tunnel) will be referred to as the ion shielding region. At large recession depths (*i.e.* h < - 7 mm), for both collectors at 500 mT, the collector voltage becomes nearly constant. This could be due to both ion and electron currents being substantially reduced by the magnetic field and surface losses resulting in a near constant collector voltage. For the intermediate field of 250 mT there is a minimum of V_C at h = - 7 mm for both collectors. At deeper recession depths V_C is seen to increase slightly with h. This could be a result of partial magnetic shielding of the ions with the electrons being almost fully shielded at this distance. Only those ions energetic enough can reach the collector causing V_C to increase at a reduced rate.

The floating potential of the fully extended collector (*i.e.* h = 5 mm) has increased from a minimum value at 8 mT indicating an increase in the plasma potential. For $B \geq 81$ mT, and as the collector is retracted (from h = 5 mm), the potential decreases, forming a potential dip, before increasing towards the plateau. The dip width is larger than the conical height of 1.5 mm and is more pronounced for the flat collector. A similar feature was also observed by Adámek *et al.* (2013) and Bousselin *et al.* (2013) but not by Zanáška *et al.* (2015). By observing the dip width to increase with λ_{De} (as the magnetic field is increased) Bousselin *et al.* (2013) attributed the dip to the expanding sheath surrounding the BPP. However, no such dip is seen for weak magnetic fields (*i.e.* B < 81 mT) outside the tunnel (see figures 5a and 5b) and there is no clear correlation with λ_{De} (see table 2). The potential dip is also seen inside the tunnel for weak magnetic fields. The potential minimum moves towards the plasma as the field is increased. Outside the tunnel (for $B \geq$ 81 mT) the potential minimum also shifts to higher h with increasing magnetic field (from h = 1 mm at 81 mT to h = 3 mm at 500 mT). It is likely that as the magnetic field is increased the potential dip first develops inside the tunnel, as a result of magnetic shielding of the electrons. As the field is increased the shielding intensifies and the dip moves towards the plasma eventually being outside the tunnel. For the conical collector significant change to the potential (whether increasing or decreasing) occurs at h = 2 mm for all field strengths. This difference in behaviour may be due to the collector geometry with the conical collector confining the electron shielding region closer to the tunnel entrance. With reference to figures 5a and 5b it can be seen that the span in V_C, for all field strengths, is smaller for the conical collector possibly due to the difference in collector geometry.

4.2.2 Current - voltage (IV) scans Swept voltage ramps, ranging from - 50 V to + 50 V, were applied to the collector and the current measured. This was done using a Hiden Langmuir probe acquisition system (ESPion) directly connected to the collector. Figure 6a shows the IV characteristics for the 2 mm ball pen probe with conical collector at 0 mT. It was not possible to acquire scans at collector depths of h < - 3 mm due to the increased noise. The minimum voltage indicates the floating potential. Because of the lower input impedance of the Hiden unit (less than 1 kΩ depending on current range) it was necessary to shift the IV curves to match the floating potentials obtained using the op-amp. At all positions the electron current is larger than the ion current. Neither ion nor electron current saturates and the currents increase with voltage. As the collector is retracted inside the tunnel both the electron current (at large positive bias) and the ion current (at large negative bias) decrease. Furthermore, the electron current decreases faster than the ion current. This causes the IV characteristic to be more symmetric. This is inconsistent with the theory developed in section 2. For the collector potential to decrease the ion current must decrease at a rate faster than the electron current. This apparent disagreement may be due to the perturbing effect of large voltages (relative to the floating potential) on the collector inside the tunnel. The collector has a similar cross-sectional area to the tunnel facilitating a large current drain. Figure 6b shows IV characteristics for the 2 mm flat collector at 81 mT. The IV

curves have again been shifted to match the floating potentials obtained with the op-amp. The IV curves are similar to those at 0 mT. Both ion and electron currents are not saturated, being highly non-linear and become increasingly symmetric with depth. Figure 7 shows the natural logarithm of both ion and electron currents (at ± 50 V) with retraction depth for the 2 mm conical ball pen probe at 0 and 81 mT. Both ion and electron currents decrease exponentially with increasing depth with regression fit values (R^2) better than 0.9. Similar behaviour and R^2 values have been obtained for the other ball pen probes. The exponential decrease of current with depth supports the assumption used in the theory (see section 2).

In high temperature fusion plasmas, the IV curves can be used to obtain α values (see equation 1). This is obtained by taking the ratio of the extrapolated electron and ion saturation currents at the collector potential. This then allows the plasma potential to be obtained if the electron temperature is known *a priori*. In these plasmas, non-saturation of the current for both species is observed but the increase is linear with applied bias voltage. The saturation currents at the floating potential can then be obtained by a linear fit to the data. The highly non-linear variation of collector current with applied voltage, as shown in figure 6b, has also been observed in magnetised low temperature plasmas by Adámek *et al.* (2013) and Zanáška *et al.* (2015). This method of estimating α is not applicable for these plasmas. A complete understanding of the IV non-linearity is required in order to determine the true ratio of the currents at floating potential.

4.2.3 Ball pen probes: diameter 4 mm Retraction scans at increasing field strengths for the 4 mm diameter collectors (flat and conical) are shown in figures 8a and 8b. Plasma conditions are the same as for the 2 mm collectors (*i.e.* 0.45 Pa and 10 W). The general behaviour of the collector potential with retraction depth and magnetic field is

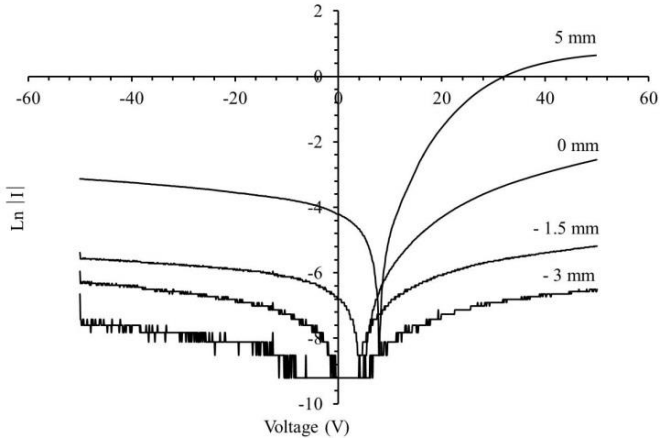

Figure 6a Collector current – voltage scans at different retraction depths at 0 mT. The ball pen probe of 2 mm diameter with a conical collector was used at 0.45 Pa and 10 W in argon.

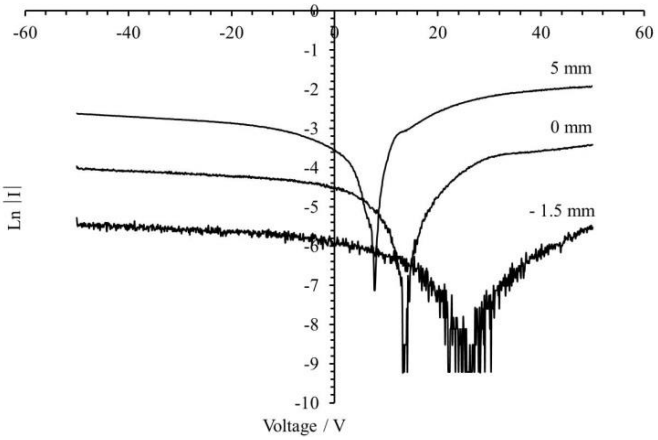

Figure 6b Collector current – voltage scans at different retraction depths at 81 mT. The ball pen probe of 2 mm diameter with a flat collector was used at 0.45 Pa and 10 W in argon.

essentially the same as for the smaller BPPs. Namely, the collector potential (and plasma potential) outside the tunnel first decrease to a minimum at 8 mT before increasing. The span of the conical collector potential (no data was obtained at 3 mT and 8 mT) is smaller than for the flat collector. Inside the tunnel the collector potential decreases for $B \leq 8$ mT and then increases for 3 mT and 8 mT. For $B \geq 81$ mT the collector potential increases to a plateau region (at 81 mT) or a broad peak ($B \geq 250$ mT). There are noticeable differences between the 2 mm and 4 mm diameter BPPs. For the 4 mm flat collector (figure 8a) the collector potential is approximately constant for $h > 2$ mm, with no potential dip, for all field strengths. For the 4 mm conical collector (figure 8b) a small potential dip is seen only at 250 mT and V_C decreases with increasing h at 500 mT. The potential dip may

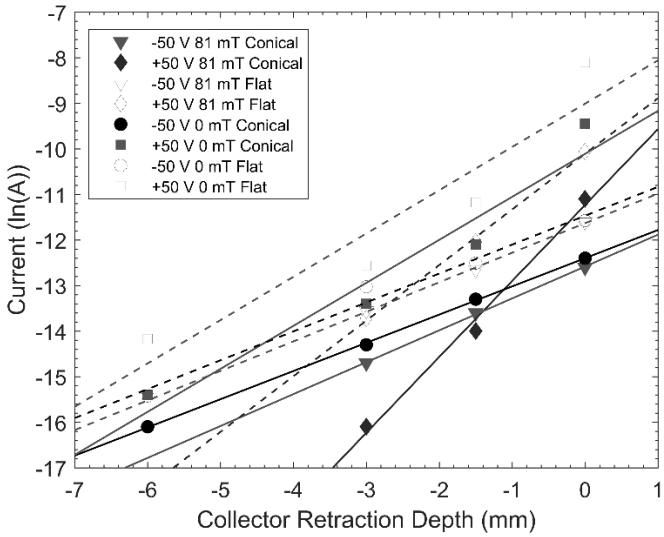

Figure 7. Conical ball pen probe (2 mm diameter) collector current at ± 50 V at different retraction depths for 0 and 81 mT.

then be more pronounced for the smaller sized collectors (see figure 5 and Bousselin *et al.* (2013)). Unlike the 2 mm BPP the potential for the conical collector increases with h for h > 3 mm at 0 mT. This is possibly due to the greater perturbing effect of the larger sized conical collector.

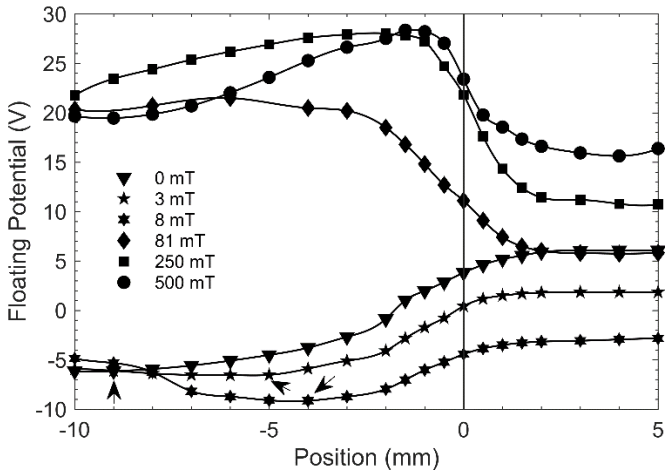

Figure 8a Axial scans for the 4 mm diameter flat collector at 0.45 Pa and 10 W in argon. Arrows indicate positions of potential minimum.

Inside the tunnel for B ≤ 8 mT, for both collectors, the potential gradient is significantly less than the 2 mm BPPs. For example, at 0 mT the potential minimum has shifted further down the tunnel by 3 mm for both 4 mm collectors. As for the 2 mm BPPs the position of the minimum then moves towards the plasma from h = - 9 mm (flat, 0 mT) to h = - 4 mm (8 mT). The total drop in potential from h = 5 mm to h = - 10 mm is significantly greater for the larger BPPs. This difference roughly doubles from 6.47 V (2 mm flat, 0

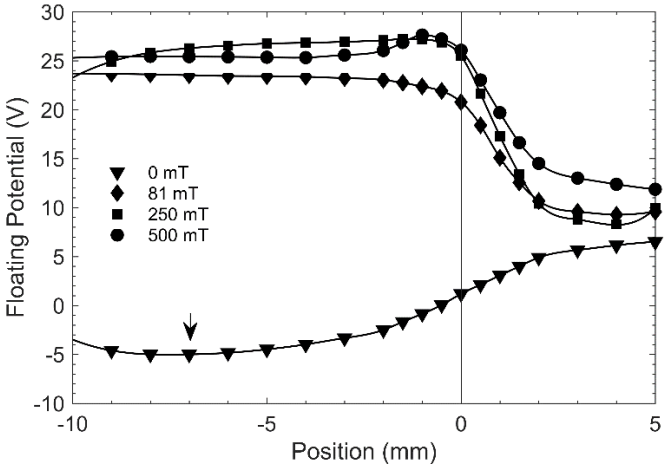

Figure 8b Axial scans for the 4 mm diameter conical collector at 0.45 Pa and 10 W in argon. Arrow indicates position of potential minimum.

mT) to 11.68 V (4 mm flat, 0 mT). Similar behaviour is also observed for the conical collector. The floating potential for the flat collectors at h = 5 mm decreases only by 0.8 V. This small change in plasma conditions does not account for the large drop in voltage. The increase of potential from 0 mT to 8 mT, at large retraction depths, is also less than the 2 mm BPPs. In figure 9 the gradient dV_C / dh and δ_e, in the electron screening region for B ≥ 81 mT, are shown for the 2 mm and 4 mm conical BPPs. It is clear that the larger BPP has the smaller gradient (and larger δ_e) for all field strengths. The corresponding δ_i for both BPPs (2 mm: δ_i = 1.54 mm; 4 mm: δ_i = 1.43 mm) are also larger than δ_e consistent with the theory. Similar conclusions were also obtained for the flat BPPs. These differences between two different tunnel sizes are due to the greater plasma penetration into the larger BPPs. This is because the effective area at the tunnel entrance, $A_{eff} = \pi[D - 2S(\lambda_{De}, B)]^2 / 4$, has increased. Here, $S(\lambda_{De}, B)$ represents the sheath width adjacent to the tunnel wall which repels (screens) electrons from entering the tunnel. This can be several to tens of λ_{De} thick depending on plasma conditions and magnetic field. Consequently, more electrons reach the collector at deeper retraction depths. This lowers the collector potential and shifts the potential minimum further into the tunnel. This effect can be seen, without magnetic field, in figures 5 and 8 for both collectors. In the electron screening region, and for B ≥ 81 mT, more electrons are able to enter the tunnel increasing the attenuation distance, δ_e. This suggests that the smaller BPP is more effective in screening electrons leading to a steeper gradient with smaller δ_e. Similar results were found by Bousselin *et al*. (2013) (see figure 5 in their paper). Electron screening is then determined by the tunnel size, the sheath width at the tunnel entrance as well as magnetic field strength. Optimum electron screening, in terms of the tunnel diameter, would be achieved when the electron repelling

sheath, from around the wall's circumference, overlap. From table 2 the ratio λ_{De} / R_D (with R_D = D / 2) increases from 0.04 (at 81 mT) to 0.15 (at 500 mT) for the 2 mm diameter BPP. Given that the sheath thickness can be up to 10 λ_{De} (depending on magnetic field and voltage drop) then the wall sheath can be a substantial fraction of the tunnel inner diameter. A maximum in dV / dh for both collectors is clearly observed at 250 mT in figure 9. Electron screening is then most effective at 250 mT for these BPPs and plasma conditions. There is no correlation with the electron Debye length as it continually increases from 81 mT to 250 mT. However, the dependence of the tunnel sheath width on the magnetic field is unknown so it is not possible to determine A_{eff}. At 500 mT the gradient has decreased so the electron screening is less effective despite the increased magnetic field. A slight kink in V_C at h = 0 mm is seen for the flat collector at 81 mT and 250 mT. No kink is observed for the conical collector for B ≥ 81 mT. This is because of the larger tunnel diameter causing less of a potential perturbation at the tunnel entrance. As noted earlier such kinks and potential dips at the tunnel entrance are more pronounced for smaller diameter tunnels.

The large decrease of V_C after the potential maximum for B ≥ 81 mT, as observed for both 2 mm BPPs, is not seen for the 4 mm BPPs. This could be due to the larger A_{eff} increasing the plasma penetration into the tunnel. This lengthens the plateau region to at least h = - 10 mm at 81 mT and broadens the peak at 250 mT and 500 mT. Note that for the 4 mm conical collector the decrease of V_C into the tunnel, after the maximum, is less rapid than the 4 mm flat collector at these field strengths. This can be attributed to the conical geometry possibly due to the stronger electric field at the tip extending the plateau region deeper into the tunnel.

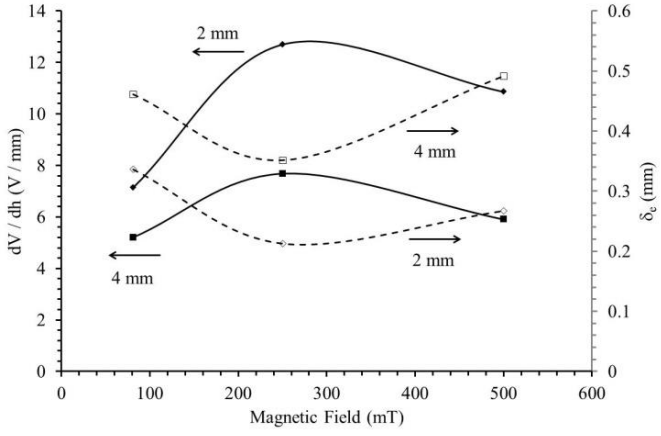

Figure 9 Electron screening region potential gradient (dV_C / dh) and electron attenuation distance (δ_e) for the conical ball pen probe (0.45 Pa and 10 W in argon).

4.3. PIC code results Particle-In-Cell simulations of the 2 mm flat collector were carried out using the model developed by Murphy-Sugrue *et al* (2017). Due to time constraints only two simulation runs were possible. Simulations were run for a unmagnetised Maxwellian DC plasma and at 250 mT. The plasma parameters are: $n_e = 10^{15}$ m^{-3}, T_e = 3 eV with room temperature ions. Note that singly charged ions were assumed with realistic ion masses for argon. The 2 mm flat BPP was operated in floating mode and the plasma potential was set to 25 V. Collisions between electrons and ions are neglected and no neutral species were included. Due to the limitations of the simulation it was not possible for the magnetic field lines to be exactly perpendicular (defined as 0° inclination angle) to the tunnel axis. The inclination angle was set to 10°. The results of these simulations, shown in figure 10, are very similar to those observed exeprimentally (see figure 5a). In the unmagnetised case the probe doesn't operate as a BPP as it is unable to effectively screen the electrons. The collector potential is constant (at 6.7 V) for h > - 1 mm (no runs were done for h > 0) and rapidly decreases to a minimum of 3.64 V at h = - 4 mm before increasing slowly. This behaviour is in good agreement with experiments. Due to the number of points it is not possible to determine the exact position of the minimum. The gradient of dV_C / dh = 1.58 V / mm gives δ_i = 1.9 mm with T_e = 3 eV. The experimental gradient is larger by a factor of 1.74 and is in good agreement with the simulation. At 250 mT the simulation shows the collector potential to rise as the collector is recessed inside the tunnel reaching a plateau for h < - 2 mm. This is different to the experimental result (figure 5a) which shows a broad peak. The start of the plateau region, between h = - 1 mm and h = - 2 mm, is in good agreement with the experimentally measured position at h = - 1.5 mm. The gradient in the electron shielding region of dV_C / dh = 19.4 V / mm is higher than the experimental value by a factor of 2.24. This is close to the factor found for the zero field case. The absence of a broad peak in the simulation could be due to the neglect of ion-neutral collisions. This would mean effects such as cross-field diffusion (which requires collisions) would be absent. This is further supported by the excellent agreement of the plateau voltage of 24.04 V to the plasma potential (of 25 V). Ion-neutral collisions, with ions losing energy, within the tunnel would be expected to decrease the collector voltage to below the plasma potential. Although the electrons are also collsionless the shift in the gyro-orbit phase (which give rise to cross-field diffusion) can occur in the electron repelling wall sheaths. The value for α, which can be estimated using equation 1, is 0.32. A low value for α is expected in a Maxwellian plasma. In real magnetised plasmas the distribution function is unlikely to be Maxwellian and so α may well be larger.

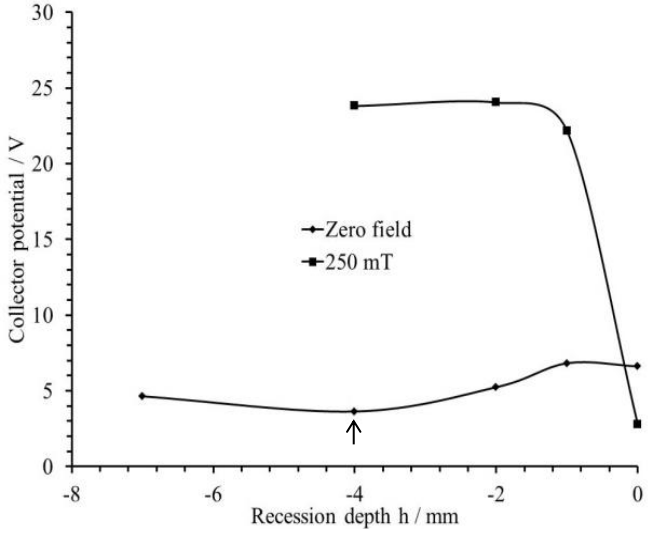

Figure 10 PIC simulations of 2 mm diameter ball pen probe with a flat collector. Arrow indicates position of potential minimum.

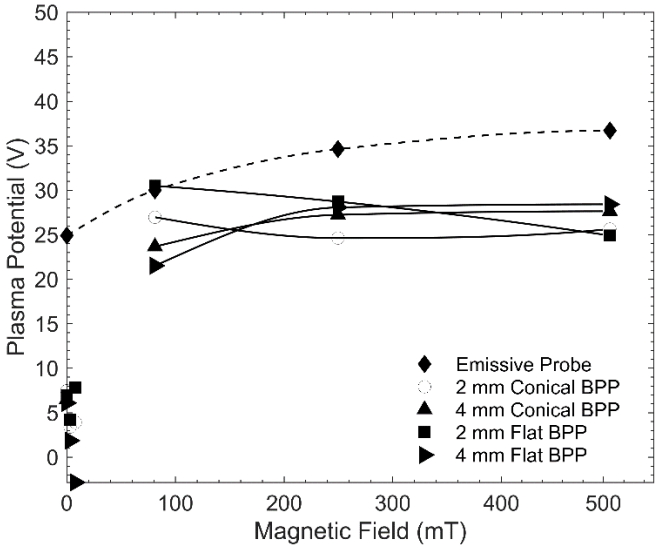

Figure 11 Comparison of emissive probe with various ball pen probes at 0.45 Pa and 10 W in argon. The 2 mm conical ball pen probe was in the same plasma as the emissive probe (open circles). The other ball pen probes were in plasmas under same conditions but without the emissive probe (filled markers).

4.4. Comparison of BPP with emissive probe In one experiment a 2 mm BPP with conical collector was compared to a 25 μm diameter emissive probe. This data is shown in figure 11 (open circles) and was taken at 0.45 Pa in increasing magnetic field. The other data (filled markers), from the 2 mm flat BPP and both 4 mm BPPs, were taken in separate experiments under the same conditions. The maximum collector potential from all BPPs was obtained from the BPP h-scans (figures 5 and 8). The emissive probe increases monotonically with magnetic field but less rapidly for $B \geq 81$ mT. Recently, Fruchtman *et al.* (2011) showed that in an unmagnetised plasma an emissive probe, in the limit of strong emission, will float about 1.5 T_e or less below the plasma potential. The upper limit of 1.5 T_e is for a planar emissive probe with smaller values depending on the parameter $\delta = \lambda_{De} / a$ (where a is the wire diameter). Computational results (figure 4 in their paper) are only shown for δ up to 2 in an argon-like plasma. From table 2 and for 0 mT $\delta = 4.83$ so that the emissive probe will float below the plasma potential by an amount less than 0.25 T_e or about 0.75 V (for $T_e = 3$ eV). However, to the authors' knowledge no such studies have been done to determine how much an emissive probe will float below the plasma potential in a magnetised plasma. Nevertheless, it is reasonable to assume that the emissive probe will float below the plasma potential by an amount less than T_e. Since the emissive probe is floating, it is expected to follow changes in the plasma potential as the magnetic field is varied.

At 0 mT the collector potentials for all BPPs are well below the emissive probe. This is because the BPPs are not in their operational range. The maximum BPP potentials correspond to either h = 5 mm or h = - 10 mm. All the BPPs are in the operational range for $B \geq 81$ mT as the electron shielding region is fully developed. The quantity $\eta = (V_E - V_{BPP}) / T_e$ gives a measure of agreement between the probes. Here, V_E and V_{BPP} refer to the emissive probe and BPP voltages respectively. The 2 mm flat BPP is in close agreement with the emissive probe at 81 mT with $\eta = -0.20$. Although this was a separate experiment the repeatability is within 1 V. The next closest agreement with the emissive probe is with the 2 mm conical BPP (with $\eta = 1.27$). Both 4 mm BPPs have $\eta \geq 2.64$. At higher field strengths all BPPs have lower potentials than the emissive probe with $\eta > 2.7$.

In figure 11, and for the 2 mm BPP flat collector, the maximum BPP potential decreases with increasing magnetic field. This is despite the increasing floating (plasma) potential at h = 5 mm (figure 5a), which is in agreement with the emissive probe. The increasing η (with $\eta > 0$) at higher fields is likely due to several competing factors. At 81 mT the electron shielding region screens out the electrons to the collector. This is most effective for the smaller BPPs with the wall sheaths being a larger fraction of the tunnel diameter. The magnetic field is weak enough so that the ions are not strongly shielded. This is characterised by a long plateau region with the energetic ions reaching the collector unimpeded. As the field increases the electron shielding is enhanced (steeper dV_c / dh) but the ions become increasingly screened from the collector. In addition, the gyration of ions around the field lines inside the tunnel causes them to be lost to the walls. The plateau evolves into a broad peak with decreasing collector potential. For the larger BPPs the screening due to the wall sheaths is less effective and a

higher magnetic field is needed to screen the electrons. This shifts the maximum collector potential to higher fields. In addition, the lower wall losses and greater plasma penetration broadens the collector peak inside the tunnel. However, at these higher field strengths the ions are increasingly screened reducing the maximum collector potential. These competing processes (electron and ion shielding) determine the maximum collector potential. For the collector to measure the plasma potential the electrons must be effectively screened but not the ions. This limits the operational range and effectiveness of the BPP.

Other processes can also lower the collector potential to below the emissive probe. Time varying rf potentials across a sheath causes an enhanced electron current to flow to the electrode or collector (Chabert and Braithwaite (2014)). This causes the floating potential V_f to shift to values lower than the plasma potential, V_p. For a planar electrode the shift in floating potential is given by $\Delta[(V_p - V_f) / T_e] = \ln [I_0(V_{rf} / T_e)]$. Here, I_0 is the modified Bessel function of zero order and V_{rf} is the rf voltage amplitude. The largest normalised difference, $\eta = 3.33$, between the emissive probe (taken to be at V_p) and the 2 mm flat BPP (at 500 mT) would require $V_{rf} = 15$ V (for $T_e = 3$ eV). This rf amplitude is comparable to those in the plasma bulk of these types of discharges. Although this may explain the disagreement at high field strengths it is inconsistent with the good agreement at 81 mT with the 2 mm flat ball pen probe.

Another possibility is ion-neutral collisions inside the tunnel or in the sheath outside the tunnel. With reference to table 2 at 0.45 Pa the ion-neutral mean free path, λ_i, is comparable to the tunnel diameter with $\lambda_i / D = 2$ ($D = 2$ mm). The loss of directional energy, as a result of a collision, would decrease the amount of charge accumulated on the collector and lower its maximum potential. However, since the ion speed inside the tunnel is not known then it is not possible to determine if collisions are important.

5. Summary and Conclusion

A theory of the ball pen probe based on exponentially decreasing ion and electron currents (characterised by their attenuation distances, δ_i and δ_e respectively) was developed. Effects such as wall losses and magnetic fields can then be incorporated into the attenuation distances. For $\delta_i < \delta_e$ the ion current decreases faster than the electron current. The collector potential then decreases with increasing depth inside the tunnel. This occurs in an unmagnetised plasma in which the accelerated ions are lost to all negatively charged surfaces in the tunnel and the electrons are repelled. In a strongly magnetised plasma the reduction in electron flux, due to cross-field diffusion and wall charging, reduces δ_e such that $\delta_e < \delta_i$, inverting the effects of the unmagnetised case. It was shown that a plateau region or a peak can only be formed inside the tunnel if $\delta_e < \delta_i$, and both vary with depth.

A comparison was made between different ball pen probes (tunnel diameters of 2 and 4 mm, flat and conical collectors) and an emissive probe. A rf driven strongly magnetised plasma (up to 500 mT) at low pressure (0.45 Pa) was used. At field strengths less than 8 mT all ball pen probes showed similar trends. At full immersion in the plasma the collector floated as a Langmuir probe. As the collector is retracted inside the tunnel the collector potential decreases, reaching a minimum value, before increasing. With increasing magnetic field the minimum moves towards the plasma and the increase of the collector potential after the minimum becomes more pronounced. This occurs when $r_{Le} \approx D$ where r_{Le} is the electron Larmor radius and D the tunnel inner diameter. This can be taken as the lower limit of ball pen probe operation. The increasing electron magnetisation reduces the collected electron current and increases the collector potential. At 81 mT and above the collector potential increases rapidly (electron shielding region) in the vicinity of the tunnel entrance. Increasing the size of the tunnel to 4 mm increases the effective area at the tunnel entrance allowing more ions and electrons to enter. For all ball pen probes a plateau region was observed only at 81 mT. At higher field strengths the plateau region develops into a broad peak of decreasing width. The decreasing collector potential after the peak (ion shielding region) is attributed to the reduction of the ion flux due to cross-field diffusion and wall losses ~~due to the gyrating ions~~. This becomes significant when $r_{Li} \approx D$. Although the ball pen continues to exhibit a maximum potential (which in fusion plasmas is close to the plasma potential) for $r_{Li} < D$ the ball pen is not expected to be within its operation range if $r_{Li} << D$. In such strong fields the ion flux is significantly reduced and the BPP will severely underestimate the plasma potential. Conical ball pen collectors were found to have a longer plateau region at 81 mT and a flatter (and wider) peak at higher field strengths.

A PIC simulation was compared to the ball pen retraction scan for the 2 mm flat collector at 0 mT and 250 mT. Good overall agreement was obtained with the experimental scans. Noticeable differences were the absence of the potential dip region in front of the tunnel (observed for small BPPs) and the broad peak (observed for $B \geq 250$ mT). Excellent agreement of the maximum collector potential with the plasma potential was found. This does not agree with the experimental result with the collector potential significantly lower than the emissive probe. However, non-Maxwellian distribution functions, time varying electric fields (found in rf plasmas) and ion-neutral collisions were not considered in the model. Further simulation work, accounting for these effects, are necessary to determine the accuracy of the BPP in rf and weakly collisional plasmas.

Within the operational range ~~of the ball pen probes~~, at field strengths greater than 81 mT, all probes underestimated the potential of a floating emissive probe by > 2.7 T_e. In a magnetic field the amount by which an emissive probe floats below (but tracks) the plasma potential is not known. The increasing discrepancy between both probes with increasing magnetic field might also be due to the limitations of the ball pen probe. Good agreement to within 0.5 T_e was obtained only with the 2 mm flat ball pen probe at 81 mT. To measure the plasma potential the magnetic field must be strong enough to screen out the electrons, but not too strong so that ions are allowed to pass. At low plasma densities or for smaller diameter tunnels the wall sheaths can occupy a significant part of the tunnel cross-section, enhancing electron screening. Other possibilities for the disagreement with the emissive probe, such as rf self-biasing and ion-neutral collisions, were shown to be possible.

In fusion plasmas the electron Debye length is of the order of 10s μm. The effective tunnel area is then approximately $A_{eff} \approx \pi D^2 / 4$ (D typically is several mm) so that the plasma penetrates the tunnel. Electron screening due to overlapping sheaths is not possible. Furthermore, both electrons and ions flow along the field lines, perpendicular to the ball pen tunnel axis, with ion velocities of 100s km / s. The tunnel diameter must then be large enough to give sufficient time for the ions to reach the recessed collector (usually $h = r_{Li}$). This condition is expressed as $v_\perp > v_{||} (h / D)$ with $v_{||}$ and $v_\perp$ the parallel and perpendicular velocities to the field. For 30 eV hydrogen ions the thermal velocity is 86 km / s. Assuming that $E_\perp = 5$ kV / m (Murphy-Sugrue *et al.* (2017)), this gives a drift velocity of 10 km/s at 0.5 T, suggesting the thermal velocity largely determines the ion speed along the tunnel axis. The condition above then reduces to the requirement $D > h (\approx r_{Li})$.

The ball pen probe operational mode is different in low temperature magentised plasmas. The electron Debye length ranges from 10 to 100s μm so that the sheath can be a substantial fraction of the tunnel radius. The lower ion temperature of around 0.025 eV allows positive ions to be more influenced by the sheath in front of the tunnel and are directed along the tunnel axis. For a planar collisionless sheath in an unmagnetised argon plasma the ion energy at the floating wall is about 5 T_e (for initially cold ions). With T_e = 3 eV this gives a velocity of about 8.5 km / s. Assuming similar velocities can be reached in a magnetised plasma and for similar inner tunnel wall electric fields of 5 kV / m at 0.5 T, the ion velocity due to sheath acceleration is compariable to the $E_\perp \times B$ drift velocity of about 10 km / s. In the case that the $E_\perp \times B$ velocity dominates the axial velocity it is easy to show that $D > (8 / \pi) T_i / E_\perp$. The high axial velocity causes the ions to penetrate further into the tunnel leading to longer plateaus. Effective screening of plasma electrons is achieved by choosing a suitably small tunnel diameter such that λ_{De} / D is sufficiently large (for significant wall sheath area). Magnetic field strengths should be strong enough so that $r_{Le} < D$ but not so strong that $r_{Li} << D$. The present study shows that further work is necessary in order to understand the limits of operation as well as the optimum design for accurate plasma potential measurements in magnetised low temperature plasmas.

Acknowledgements

The authors wish to acknowledge the EPSRC research council for the funding of this project (under grant EP/M001709/1). Also, the authors wish to thank Mr Gareth Blacoe for construction of the emissive and ball pen probes.

References

Adámek J, Horacek J, Seidl J, *et al.* 2014 *Contributions to Plasma Physics* **54** 279

Adámek J, Peterka M, Gyergyek T, *et al.* 2013 *Contrib. Plasma Phys.* **53** 39

Adámek J, Peterka M, Gyergyek T, *et al.* 2012 *Nukleonika* **57** 297

Adámek J, Rohde V, Müller H W, *et al.* 2009 *Journal of Nuclear Materials* **390-391** 1114

Adámek J, Stöckel J, Ďuran I, *et al.* 2005 *Czech. J. Phys.* **55** 235

Adámek J, Stöckel J, Hron M, *et al.* 2004 *Czech. J. Phys.* **54** C95

Bousselin G, Cavalier J, Pautex J F, *et al.* 2013 *Rev. Sci. Instrum.* **84** 013505

Chabert P and Braithwaite N St J 2014 *Physics of Radio-frequency Plasmas* (Cambridge University Press)

Costea S, Fonda B, Kovačič J, *et al.* 2016 *Rev. Sci. Instrum.* **87** 053510

Cullen P J and Milosavljević V 2015 *Prog. Theor. Exp. Phys.* 063J01

Du B, Celik Y, Luggenhölscher D and Czarnetzki U 2010 *Plasma Sources Sci. Technol.* **19** 045008

Elmore S, Allan S Y, Kirk A, *et al.* 2012 *Plasma Phys. Control. Fusion* **54** 065001

Fantz U 2006 *Plasma Sources Sci. Technol.* **15** S137–S147

Fruchtman A, Zoler D and Makrinich G 2011 *Phys. Rev. E* **84** 025402

Grover O, Adámek J, Seidl J, *et al.* 2017 *Rev. Sci. Instrum.* **88** 063501

Horacek J, Adámek J, Müller H W, *et al.* 2010 Nucl. Fusion **50** 105001

Lieberman M A and Lichtenberg A J 1994 *Principles of Plasma Discharges and Materials Processing* (Wiley: New York)

McDaniel E W and Mason E A 1970 *The Mobility and Diffusion of Ions in Gases* (Wiley: New York)

McWhirter R W P, 1965 *Plasma Diagnostic Techniques* (Ed. Huddlestone R H and Leonard S L: Academic) 201–261

Meshkani S, Ghoranneviss M, Elahi A S, *et al.* 2015 *J. Fusion Energ.* **34** 394

Müller H W, Adámek J, Cavazzana R, *et al.* 2011 *Nucl. Fusion* **51** 073023

Michael C A, Zhao F, Blackwell B, *et al*. 2017 *Plasma Phys. Control. Fusion* **59** 024001

Mishra A, Kelly P J and Bradley J W 2010 *Plasma Sources Sci. Technol.* **19** 045014

Murphy-Sugrue S, Harrison J, Walkden N R, *et al.* 2017 *Plasma Phys. Control. Fusion* **59** 055007

Sheehan J P and Hershkowitz N 2011 *Plasma Sources Sci. Technol.* **20** 063001

Silva C, Adámek J, Fernandes H and Figueiredo H 2015 *Plasma Phys. Control. Fusion* **57** 025003

Sykes A, Akers R J, Appel L C, *et al.* 2001 *Nuclear Fusion* **41** 1423

Walkden N R, Adámek J, Allan S, *et al.* 2015 *Rev. Sci. Instrum.* **86** 023510

Zanáška M, Adámek J, Peterka M, *et al.* 2015 *Phys. Plasmas* **22** 033516